

Bifurcation-based adiabatic quantum computation with a nonlinear oscillator network: Toward quantum soft computing

Hayato Goto

*Frontier Research Laboratory, Corporate Research & Development Center,
Toshiba Corporation, 1, Komukai Toshiba-cho, Saiwai-ku, Kawasaki-shi, 212-8582, Japan*

The dynamics of nonlinear systems qualitatively change depending on their parameters, which is called bifurcation. A quantum-mechanical nonlinear oscillator can yield a quantum superposition of two oscillation states, known as a Schrödinger cat state, via its bifurcation with a slowly varying parameter. Here we propose a quantum computer comprising such quantum nonlinear oscillators, instead of quantum bits, to solve hard combinatorial optimization problems. The nonlinear oscillator network finds optimal solutions via quantum adiabatic evolution, where nonlinear terms are increased slowly, in contrast to conventional adiabatic quantum computation or quantum annealing. It is notable that the present computer is analogous to neural computers, which are networks of nonlinear components. Thus, the present scheme will open various possibilities for quantum computation, nonlinear science, and artificial intelligence.

Nonlinearity is the origin of various interesting phenomena, such as chaos, fractal, and bifurcation [1]. A bifurcation is a parameter-dependent qualitative change in nonlinear dynamics, such as a transition from a single stable state to two stable ones (bistability). As a result of recent advances in nanotechnology, artificial nonlinear oscillators may possess large nonlinearity and low loss simultaneously and consequently enter the quantum regime [2]. A remarkable example is the generation of a quantum superposition of two oscillation states, known as a Schrödinger cat state, with superconducting microwave resonators coupled to a superconducting artificial atom [3], where nonlinear dissipation exceeds linear one. Here we first show that a quantum-mechanical nondissipative oscillator with desirable nonlinearity can yield a cat state via its bifurcation with a slowly varying parameter. Next, we propose a quantum computer comprising such quantum nonlinear oscillators, which exploits a superposition of an exponentially large number of states of the nonlinear oscillator network to solve combinatorial optimization problems. The nonlinear oscillator network finds optimal solutions via quantum adiabatic evolution, as conventional adiabatic quantum computation [4] or quantum annealing [5–7] does. However, these mechanisms are different: whereas in quantum annealing quantum fluctuation terms are decreased slowly, in the present computation nonlinear terms are increased slowly. To distinguish them, we refer to the present approach as bifurcation-based adiabatic quantum computation. Finally, we present numerical simulation results indicating that quantum superposition and quantum fluctuation work effectively in the computation.

We start with a single quantum nonlinear oscillator. The oscillator used here is a parametrically driven Kerr (or Duffing) nonlinear oscillator (KPO). In a frame rotating at half the pump frequency of the parametric drive and in the rotating-wave approximation, its Hamiltonian is

$$H_1 = \hbar\Delta a^\dagger a + \hbar\frac{K}{2}a^{\dagger 2}a^2 - \hbar\frac{p}{2}(a^{\dagger 2} + a^2), \quad (1)$$

where a and a^\dagger are the annihilation and creation operators for quanta of the oscillator (the quanta are, e.g., photons for electromagnetic resonators or phonons for mechanical oscillators), Δ is the detuning of the oscillator eigenfrequency from half the pump frequency, K is the Kerr coefficient for the Kerr effect, and p is the pump amplitude for the parametric drive [2]. This is the simplest model necessary and sufficient for the present purpose. This model is also physically feasible. Promising candidates for implementing this model are superconducting microwave resonators with Josephson junctions [3, 8, 9] (Chap. 15 in [2]), nanoelectromechanical systems [10, 11] (Chap. 10 in [2]), and carbon nanotubes [12] (Chaps. 12 and 13 in [2]). Hereafter, we assume that K and Δ are positive constants and p is a nonnegative control parameter. When K is negative, similar discussion is straightforward.

Before describing the quantum dynamics, we consider a classical model for the KPO. This is helpful for understanding the quantum dynamics, as found below. The classical equations of motion are

$$\dot{x} = y [\Delta + p + K(x^2 + y^2)], \quad (2)$$

$$\dot{y} = x [-\Delta + p - K(x^2 + y^2)], \quad (3)$$

where the dots denote differentiation with respect to time t . These equations are derived by replacing a with a complex number $x + iy$ in the Heisenberg equations of motion with H_1 . Here x and y are real variables corresponding to the Hermitian operators $(a + a^\dagger)/2$ and $(a - a^\dagger)/2i$, respectively, often called quadrature amplitudes.

To grasp the dynamics of such a nonlinear system, it is useful to investigate the fixed points, which are defined by $\dot{x} = \dot{y} = 0$ [1]. When $p \leq \Delta$, the origin is a single fixed point, which is stable. When $p > \Delta$, the origin becomes an unstable fixed point and two stable ones are created, the positions of which are $(\pm\sqrt{(p - \Delta)/K}, 0)$. Thus, the bifurcation point is $p = \Delta$. The dependence of the fixed points on p is depicted in Figs. 1(a) and 1(b) as the bold lines, where the solid and broken lines correspond to the stable and unstable fixed points, respectively. (In Fig.

1, Δ is set to K .) Such figures are called bifurcation diagrams [1].

The oscillating thin curves in Figs. 1(a) and 1(b) are obtained by numerically solving Eqs. (2) and (3), where $p(t)$ is increased linearly from $p(0) = 0$ to $p(500/K) = 5K$ and the initial condition is set as $x(0) = 0.1$ and $y(0) = 0$. This result suggests that when the initial state is near a stable fixed point and the pump amplitude varies slowly, the trajectory follows one of the stable branches of the bifurcation.

This result can be understood as follows. This system with constant p is conservative with the following conserved quantity:

$$E(x, y) = \frac{\Delta}{2} (x^2 + y^2) + \frac{K}{4} (x^2 + y^2)^2 - \frac{p}{2} (x^2 - y^2).$$

Thus, the trajectories are given by contours of $E(x, y)$ [1]. Examples of the trajectories are shown in Figs. 1(c) ($p = 0.9\Delta$) and 1(d) ($p = 3\Delta$), where filled and open circles represent stable and unstable fixed points, respectively. (Such figures are called phase portraits [1].) In the above simulation, the trajectory is initially a small closed orbit around the origin. As p is increased slowly, the orbit changes while keeping its area $\int dx dy$ constant according to the adiabatic theorem in classical mechanics, where the area is called adiabatic invariance [13]. Thus, above the bifurcation point ($p > \Delta$), the orbit moves to one of the stable fixed points (local minima of the energy surface).

Here we move on to the quantum dynamics of the KPO. We numerically solved the Schrödinger equation with H_1 , where the Hilbert space was truncated at a “photon” number of 20, the initial state was set to the “vacuum” $|0\rangle$, and p was increased linearly from zero as in the above classical simulation. Figures 1(e) and 1(f) show the Wigner function $W(x, y)$ at $p = 0.9\Delta$ and $p = 5\Delta$, respectively, where the Wigner function is a quasiprobability distribution for quadrature amplitudes [14] (also see Appendix A). In Figs. 1(e) and 1(f), filled and open circles represent classical stable and unstable fixed points, respectively, as in Figs. 1(c) and 1(d). Note that the peaks of the Wigner function are at the classical stable fixed points. The Wigner distributions show that the stable fixed points are accompanied by quantum fluctuations due to the Heisenberg uncertainty relation. On the other hand, the interference fringe between the two peaks in Fig. 1(f) means that the two oscillation states are superposed, that is, a cat state is generated [14]. These results suggest that the quantum dynamics may be described by a superposition of classical trajectories accompanied by quantum fluctuations.

The cat-state generation is explained by the quantum adiabatic theorem as follows. The initial state $|0\rangle$ is the ground state for H_1 with $p = 0$. As p is increased slowly, the system follows adiabatically the ground state of $H_1(t)$. Finally, p becomes much larger than Δ and the final state becomes approximately the ground state of H_1 with $\Delta = 0$, which is a superposition of coherent states

$|\pm\sqrt{p/K}\rangle$ [15]. Since H_1 is symmetric under parity inversion $a \rightarrow -a$, the final state should have the same parity as $|0\rangle$. Consequently, the final state is approximately the cat state $(|\sqrt{p/K}\rangle + |-\sqrt{p/K}\rangle)/\sqrt{2}$.

Recently, deterministic cat-state generation has been demonstrated in two ways with superconducting microwave resonators coupled to a superconducting artificial atom [3, 8]. The above result provides another method for deterministic cat-state generation based on quantum adiabatic evolution.

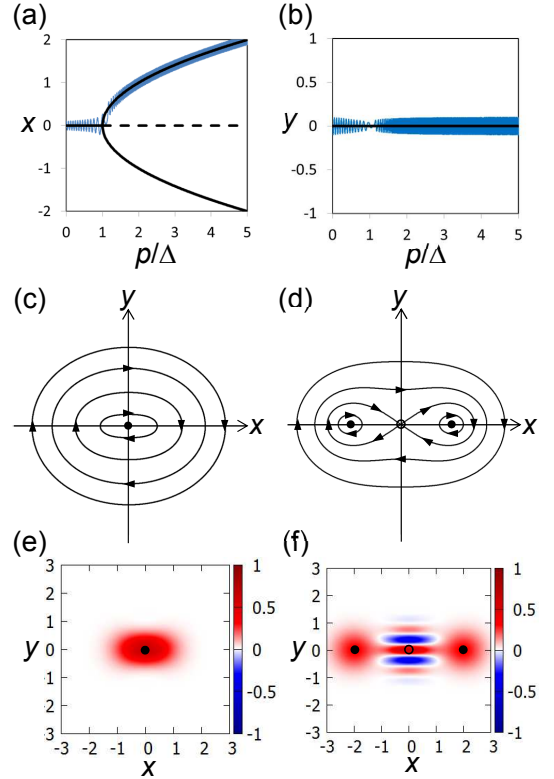


FIG. 1. Dynamics of a single KPO. Here Δ is set to K . (a) and (b) show the bifurcation diagram (bold lines) and the simulation result (thin lines) for the classical model, where the solid and broken bold lines correspond to the stable and unstable fixed points, respectively. (c) and (d) show the phase portraits for the classical model, where $p = 0.9\Delta$ in (c) and $p = 3\Delta$ in (d). (e) and (f) show the Wigner functions obtained by numerically solving the Schrödinger equation with H_1 in Eq. (1), where $p = 0.9\Delta$ in (e) and $p = 5\Delta$ in (f). In (c)–(f), the filled and open circles represent the classical stable and unstable fixed points, respectively.

Next, our quantum computer with KPOs is described. The objective is to solve a combinatorial optimization problem known as the Ising problem: given a dimensionless Ising energy

$$E_{\text{Ising}} = -\frac{1}{2} \sum_{i=1}^N \sum_{j=1}^N J_{i,j} s_i s_j, \quad (4)$$

we want to find the spin configuration minimizing E_{Ising} .

Here the Ising spin s_i takes ± 1 , N is the number of spins, and the coupling coefficients satisfy $J_{i,i} = 0$ and $J_{i,j} = J_{j,i}$. This Ising problem is very hard (unless the coupling topology is too simple); more precisely, is known to be a non-deterministic polynomial-time hard (NP-hard) problem in computational complexity theory [16]. Recently, machines specially designed for the Ising problem have attracted much attention [17–24].

For the above problem, N KPOs are prepared and coupled to one another to realize the following total Hamiltonian:

$$H = \sum_{i=1}^N H_1^{(i)} - \hbar \frac{\xi_0}{2} \sum_{i=1}^N \sum_{j=1}^N J_{i,j} (a_i^\dagger a_j + a_i a_j^\dagger), \quad (5)$$

where $H_1^{(i)}$ is the Hamiltonian for the i th KPO of the form of Eq. (1) with an individually controllable detuning Δ_i and ξ_0 is a positive constant with the dimension of frequency. Note that the coupling Hamiltonian describes standard linear couplings, and therefore is physically fea-

sible.

To use a quantum adiabatic evolution and to find the configuration minimizing E_{Ising} , the initial state $|0\rangle$ should be the ground state of H with $p = 0$. This condition can be satisfied by setting the detunings such that the following matrix M becomes nonnegative definite (see Appendix C for the proof):

$$M_{i,i} = \Delta_i, \quad M_{i,j} = -\xi_0 J_{i,j} \quad (i \neq j). \quad (6)$$

A simple setting satisfying this condition is as follows (see Appendix C):

$$\Delta_i = \xi_0 \sum_{j=1}^N |J_{i,j}|. \quad (7)$$

By increasing p slowly, we obtain the ground state of H with large p . When p is much larger than $|\Delta_i|$ and $\xi_0 |J_{i,j}|$, the nonlinear terms in H are dominant and each KPO becomes $|\pm \sqrt{p/K}\rangle$, as in the case of a single KPO. Thus, the final state is of the following form:

$$|\psi_f\rangle = \frac{|s_1 \sqrt{p/K}\rangle \cdots |s_N \sqrt{p/K}\rangle + |-s_1 \sqrt{p/K}\rangle \cdots |-s_N \sqrt{p/K}\rangle}{\sqrt{2}}, \quad (8)$$

where $s_i = \pm 1$ and the parity symmetry of H has been taken into account, as in the case of the cat-state generation presented above. The values of $\{s_i\}$ are determined such that the following final energy becomes minimal:

$$E_f = \langle \psi_f | H | \psi_f \rangle = \sum_{i=1}^N \hbar \left(\Delta_i \frac{p}{K} - \frac{p^2}{2K} \right) - \hbar \xi_0 \sum_{i=1}^N \sum_{j=1}^N J_{i,j} s_i s_j \frac{p}{K}, \quad (9)$$

where $|\langle \sqrt{p/K} | -\sqrt{p/K} \rangle| = e^{-2p/K}$ has been neglected assuming sufficiently large p . Note that $\{s_i\}$ minimizing E_f is the same as that minimizing E_{Ising} . Thus, we can find the solution of the Ising problem by measuring the quadrature amplitudes of the KPOs and identifying their signs with the Ising spins.

Here it is notable that an entangled cat state given by Eq. (8) is generated as a result of the quantum computation. We confirmed this fact by numerical simulation in the case of two spins (see Appendix D). Thus, the present scheme provides a method for the generation of the intriguing states via quantum adiabatic evolution.

Finally, we present numerical simulation results of the quantum computation for four-spin problems, which are more difficult than two- and three-spin ones in the sense that, in the four-spin case, there may be not only frustration but also a local minimum that is not a global minimum. In these simulations, the Schrödinger equation with H in Eq. (5) is numerically solved, where the Hilbert space is truncated at a “photon” number of 16 for each KPO, the initial state is set to $|0\rangle$, $\xi_0 = 0.5K$, the detunings are set as in Eq. (7), and p is increased linearly from $p(0) = 0$ to $p(700/K) = 7K$.

We generated 1000 instances of the problem with the coupling coefficients chosen randomly from -1 to 1 . We

estimated the success probability and the residual energy for each instance [see Appendix B for details], where the residual energy is defined as the difference between the Ising energy obtained by simulation and its minimum value [6]. The histograms of the success probabilities and the residual energies are shown in Figs. 2(a) and 2(b), respectively. In Fig. 2, we treat the two configurations $\{s_i\}$ and $\{-s_i\}$ as a pair because these configurations give the same value of E_{Ising} .

We also simulated a classical model for the quantum computation, the equations of which are derived in a similar manner to Eqs. (2) and (3) (see Appendix E). From the results for a single KPO, it is expected that the classical simulation will be helpful for grasping the present dynamics. For each instance, we repeated the simulation 100 times, setting the initial values of x_i and y_i to random numbers from -10^{-6} to 10^{-6} . The success probability and the residual energy for each instance are estimated by taking averages. The results are shown in Figs. 2(c)

and 2(d).

First, it is notable that the classical model can find the global minimum with high probability. This result comes from that the classical model can solve a relaxation problem of the Ising problem [25]. The high success probability for the classical model means that an approximation based on the relaxation is fairly good.

Next, the quantum model can achieve higher performance than the classical one for both the success probability and the residual energy. Since the differences between the two models are quantum superposition and quantum fluctuation, as mentioned above, the high performance may come from these quantum effects. To examine this point, we look into one of the most difficult instances, for which the classical model almost always failed. The results are shown in Figs. 2(e) and 2(f). Figure 2(g) shows the energy landscape of this instance, where the distance between a configuration $\{s_i\}$ and the solution $\{S_i\}$ is defined as

$$D(\{s_i\}, \{S_i\}) = \min \left(\sum_{i=1}^4 |s_i - S_i|/2, 4 - \sum_{i=1}^4 |s_i - S_i|/2 \right). \quad (10)$$

In this problem, there are two local minima and the eigenvector of M for the smallest eigenvalue corresponds to the one that is not a global minimum. Thus, the classical model is trapped around the local minimum [Fig. 2(f)]. On the other hand, in the quantum model, the system becomes a superposition of the two local minima because of quantum fluctuations, and finally arrives at the global minimum via quantum adiabatic evolution. Thus, we conclude that the quantum effects work effectively, as expected.

In conclusion, we have proposed a quantum computer comprising quantum nonlinear oscillators exhibiting quantum mechanical bifurcation. The quantum computer solves combinatorial optimization problems via quantum adiabatic evolution, where nonlinear terms are increased slowly. Since this mechanism is different from that of conventional adiabatic quantum computation or quantum annealing, where quantum fluctuation terms are decreased slowly, we refer to the present approach as bifurcation-based adiabatic quantum computation. By simulating four-spin Ising problems and comparing the results with those for a classical model, we have concluded that quantum superposition and quantum fluctuation work effectively. While conventional quantum computers with quantum bits and quantum gates [26, 27] are analogous to current digital computers with bits and logic gates, the present one is analogous to neural computers [28], which are networks of nonlinear components, like a brain [29]. Thus, the present scheme will lead to the emergence of a new paradigm, which may be called “quantum soft computing,” in the fields of quantum information, nonlinear dynamics, and artificial intelligence.

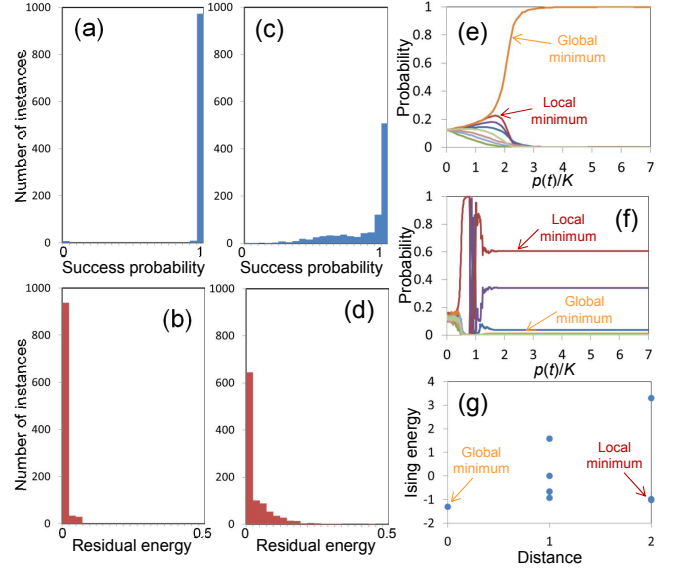


FIG. 2. Simulation results for four-spin Ising problems. (a) and (b) show the histograms for the success probabilities and the residual energies, respectively, in the quantum computation estimated by numerically solving the Schrödinger equation with H in Eq. (5). (c) and (d) show the similar results for the classical model. (e) and (f) show the time evolutions of the probabilities of the spin configurations in the quantum and classical models, respectively, for one of the most difficult instances, for which the classical model almost always failed. The energy landscape of this instance is shown in (g), where the distance is defined by Eq. (10). Here the two configurations $\{s_i\}$ and $\{-s_i\}$ are treated as a pair because these configurations give the same value of E_{Ising} .

ACKNOWLEDGMENTS

I acknowledge Koichi Mizushima for useful comments.

Appendix A: The Wigner function

The Wigner function $W(x, y)$ is a quasiprobability distribution for quadrature amplitudes, x and y , defined in the case of a single oscillator as follows [14]:

$$W(x, y) = \frac{1}{\pi} \int_{-\infty}^{\infty} e^{2iyz} \left\langle x - \frac{z}{2} \left| \rho \left| x + \frac{z}{2} \right. \right. \right\rangle dz, \quad (\text{A1})$$

where ρ is the density operator for the system and $|x\rangle$ denotes the eigenstate for $(a + a^\dagger)/2$. The Wigner function has a useful property that the integration with respect to y from $-\infty$ to ∞ gives the probability distribution for x , and vice versa. Although in the following, we focus on the case of a single oscillator, the generalization to multiple oscillators is straightforward.

Using the displacement operator $D(\alpha) = e^{\alpha a^\dagger - \alpha^* a}$ and the parity operator $P = e^{i\pi a^\dagger a}$, the Wigner function is

rewritten as follows [14]:

$$W(x, y) = \frac{2}{\pi} \text{tr} [D(2(x + iy))P\rho]. \quad (\text{A2})$$

From this formula, the Wigner function in the number representation is given by

$$W(x, y) = \frac{2}{\pi} \sum_{m=0}^{\infty} \sum_{n=0}^{\infty} (-1)^n D_{m,n}(x + iy) \rho_{n,m}, \quad (\text{A3})$$

where $\rho_{n,m}$ and $D_{m,n}(\alpha)$ are matrix elements of ρ and $D(\alpha)$, respectively, in the number representation. $D_{m,n}(\alpha)$ can be expressed as

$$D_{m,n}(\alpha) = e^{-|\alpha|^2} \sqrt{m!n!} \sum_{k=0}^{\min(m,n)} \frac{1}{k!} \frac{\alpha^{m-k}}{(m-k)!} \frac{(-\alpha^*)^{n-k}}{(n-k)!}. \quad (\text{A4})$$

We used Eqs. (A3) and (A4) for Figs. 1(e) and 1(f).

Appendix B: Calculations of success probabilities and residual energies

The success probability in Fig. 2(a) is defined as the probability that the spin configurations corresponding to the solution are obtained in the final measurement of the signs of the quadrature amplitudes. Here we explain how to calculate the probability that a spin configuration is obtained. The residual energies in Fig. 2(b) are obtained by taking expectation values with the probabilities. Although in the following, we focus on the case of a single oscillator, the generalization to multiple oscillators is straightforward.

The probability that a positive quadrature amplitude is obtained is given with the Wigner function as follows:

$$P_+ = \int_0^{\infty} dx \int_{-\infty}^{\infty} dy W(x, y) = \int_0^{\infty} r dr \int_{-\frac{\pi}{2}}^{\frac{\pi}{2}} d\phi W(r, \phi), \quad (\text{B1})$$

where we have used the polar coordinates. Using Eqs. (A3) and (A4), we obtain

$$P_+ = \sum_{m=0}^{\infty} \sum_{n=0}^{\infty} I_{m,n}^{(+)} \text{Re}(\rho_{n,m}),$$

where

$$I_{m,n}^{(+)} = \begin{cases} \frac{n!}{2} \sum_{k=0}^n \frac{(-1)^k}{k!} \frac{2^{n-k}}{(n-k)!} & \dots m = n \\ 0 & \dots m \neq n \wedge m \equiv n \pmod{2} \\ \sqrt{\frac{m!n!}{2\pi}} \frac{(-1)^{\frac{m-n-1}{2}}}{m-n} \sum_{k=0}^{\min(m,n)} \frac{(-1)^k}{k!} \frac{(m+n-2k)!!}{(m-k)!(n-k)!} & \dots m-n \equiv 1 \pmod{2} \end{cases}$$

Similarly, the probability that a negative quadrature amplitude is obtained is given by

$$P_- = \sum_{m=0}^{\infty} \sum_{n=0}^{\infty} I_{m,n}^{(-)} \text{Re}(\rho_{n,m}),$$

where

$$I_{m,n}^{(-)} = \begin{cases} \frac{n!}{2} \sum_{k=0}^n \frac{(-1)^k}{k!} \frac{2^{n-k}}{(n-k)!} & \dots m = n \\ 0 & \dots m \neq n \wedge m \equiv n \pmod{2} \\ \sqrt{\frac{m!n!}{2\pi}} \frac{(-1)^{\frac{m-n+1}{2}}}{m-n} \sum_{k=0}^{\min(m,n)} \frac{(-1)^k}{k!} \frac{(m+n-2k)!!}{(m-k)!(n-k)!} & \dots m-n \equiv 1 \pmod{2} \end{cases}$$

Appendix C: Proof of the condition for quantum adiabatic evolution

Here we prove that a sufficient condition for that $|0\rangle$ is the ground state for H with $p = 0$ is that M defined by

Eq. (6) becomes nonnegative definite.

The total Hamiltonian H with $p = 0$ can be written as

$$H = \hbar \frac{K}{2} \sum_{i=1}^N a_i^{\dagger 2} a_i^2 + \hbar \sum_{i=1}^N \sum_{j=1}^N M_{i,j} a_i^{\dagger} a_j. \quad (C1)$$

Since $H|0\rangle = 0$, it is sufficient to show that H is nonnegative.

Since M is a Hermitian matrix, M is diagonalized as $D = U M U^{\dagger}$, where D and U are a diagonal matrix and a unitary matrix, respectively. Thus we obtain

$$H = \hbar \frac{K}{2} \sum_{i=1}^N a_i^{\dagger 2} a_i^2 + \hbar \sum_{i=1}^N D_{i,i} b_i^{\dagger} b_i, \quad (C2)$$

where $b_i = \sum_{j=1}^N U_{i,j} a_j$. The operator of this form is nonnegative when K and all $D_{i,i}$ are nonnegative. All $D_{i,i}$ are nonnegative by the assumption that M is nonnegative definite. Thus, the proof is completed.

This condition is satisfied by choosing Δ_i as Eq. (7). This is easily confirmed as follows. Consider the following quadratic form of real variables $\{\eta_i\}$:

$$\sum_{i=1}^N \sum_{j=1}^N M_{i,j} \eta_i \eta_j = \xi_0 \sum_{i=1}^N \sum_{j=i+1}^N |J_{i,j}| \left(\eta_i - \frac{J_{i,j}}{|J_{i,j}|} \eta_j \right)^2,$$

where Eq. (7) has been used. This quadratic form is always nonnegative. Therefore, M is nonnegative definite.

Appendix D: Simulation of the quantum computation for a two-spin Ising problem with a ferromagnetic coupling

As a simplest problem, we considered a two-spin problem with a ferromagnetic coupling: $J_{1,2} = J_{2,1} = 1$. In this case, the answer is easy: $s_1 = s_2 = \pm 1$. From Eq. (8), we will obtain an entangled cat state:

$$|ECS(p)\rangle = \frac{|\sqrt{p/K}\rangle |\sqrt{p/K}\rangle + |-\sqrt{p/K}\rangle |-\sqrt{p/K}\rangle}{\sqrt{2}}. \quad (D1)$$

We numerically solved the Schrödinger equation with H in Eq. (5), where the Hilbert space was truncated at a “photon” number of 20 for each KPO, the initial state was set to $|0\rangle$, $\Delta_1 = \Delta_2 = \xi_0 = 0.5K$, and p is increased linearly from zero to $5K$. Figure 3 shows the fidelity between the calculated state $|\psi(t)\rangle$ and the entangled cat state $|ECS(p(t))\rangle$ defined as $F = |\langle ECS(p(t)) | \psi(t) \rangle|^2$. In Fig. 3, the upper and lower curves are the results for the computation times of $500/K$ and $200/K$, respectively.

The high fidelities in Figs. 3 prove that the entangled cat state can be generated indeed. Thus, the present quantum computation provides a simple method for deterministic generation of such an intriguing quantum state via quantum adiabatic evolution. Figure 3 also shows that the more slowly, p is increased, the higher the fidelity becomes. This is the feature of quantum adiabatic evolution.

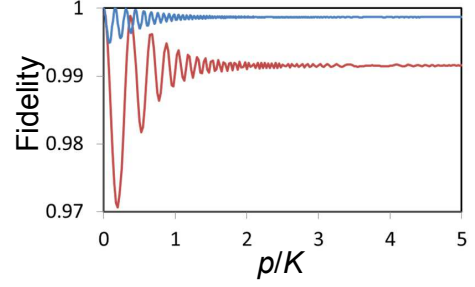


FIG. 3. Simulation result of the quantum computation for a two-spin Ising problem with a ferromagnetic coupling: $J_{1,2} = J_{2,1} = 1$. The fidelity is defined as $F = |\langle ECS(p(t)) | \psi(t) \rangle|^2$, where $|\psi(t)\rangle$ is the calculated state and $|ECS(p(t))\rangle$ is the entangled cat state defined by Eq. (D1). The parameters are set as $\Delta_1 = \Delta_2 = \xi_0 = 0.5K$. p is increased linearly from zero to $5K$. The upper and lower curves correspond to the computation times of $500/K$ and $200/K$, respectively.

Appendix E: Approximate solution by the classical model

The equations of motion in the classical model for the present quantum computation are given by

$$\dot{x}_i = y_i [\Delta_i + p + K(x_i^2 + y_i^2)] - \xi_0 \sum_{j=1}^N J_{i,j} y_j, \quad (E1)$$

$$\dot{y}_i = x_i [-\Delta_i + p - K(x_i^2 + y_i^2)] + \xi_0 \sum_{j=1}^N J_{i,j} x_j. \quad (E2)$$

Here we show that the classical model can obtain solutions for a relaxation problem of the Ising problem, where the relaxation is to replace the Ising spin s_i with a continuous variable ζ_i . We obtain an approximate solution for the original problem by identifying the sign of ζ_i as s_i .

First, we restate the Ising problem as the following energy is to be minimized:

$$\begin{aligned} E'_{Ising} &= -\xi_0 \sum_{i=1}^N \sum_{j=1}^N J_{i,j} s_i s_j + \sum_{i=1}^N \Delta_i s_i^2 \\ &= \sum_{i=1}^N \sum_{j=1}^N M_{i,j} s_i s_j. \end{aligned}$$

Since $s_i^2 = 1$, this problem is equivalent to the original one.

The relaxation problem is defined as the following energy is to be minimized under the condition that $\sum_{i=1}^N \zeta_i^2 = N$:

$$E_c = \sum_{i=1}^N \sum_{j=1}^N M_{i,j} \zeta_i \zeta_j,$$

where the constraint condition is necessary to find non-trivial solutions. Since M is nonnegative definite, the

solution of the relaxation problem is given by the eigenvector of M for the smallest eigenvalue. Here it is also important that we can obtain a lower bound for the Ising energy from the solution of the relaxation problem.

On the other hand, the classical model can find such a vector at the bifurcation point. Near the bifurcation point, the quadrature amplitudes are small. Neglecting the nonlinear terms, we obtain the following condition

for the fixed points:

$$y_i (\Delta_i + p) - \xi_0 \sum_{j=1}^N J_{i,j} y_j = p y_i + \sum_{j=1}^N M_{i,j} y_j = 0,$$

$$x_i (-\Delta_i + p) + \xi_0 \sum_{j=1}^N J_{i,j} x_j = p x_i - \sum_{j=1}^N M_{i,j} x_j = 0.$$

These are characteristic equations for M . Since M is non-negative definite and $p \geq 0$, $\{y_i\}$ cannot have nontrivial solutions. On the other hand, $\{x_i\}$ has a nontrivial solution at the bifurcation point, where p is the smallest eigenvalue of M . Then $\{x_i\}$ is the corresponding eigenvector.

Thus the classical model can find the solution for the relaxation problem of the Ising problem. This is the reason why the classical model can find optimal solutions with high probability, as shown in Fig. 2(c).

-
- [1] S. H. Strogatz, *Nonlinear dynamics and chaos* (Westview Press, Boulder, CO, ed. 2, 2015).
 - [2] M. Dykman, Ed., *Fluctuating nonlinear oscillators* (Oxford Univ. Press, Oxford, 2012).
 - [3] Z. Leghtas *et al.*, Confining the state of light to a quantum manifold by engineered two-photon loss, *Science* **347**, 853-857 (2015).
 - [4] E. Farhi *et al.*, A Quantum Adiabatic Evolution Algorithm Applied to Random Instances of an NP-Complete Problem, *Science* **292**, 472-475 (2001).
 - [5] T. Kadowaki, H. Nishimori, Quantum annealing in the transverse Ising model, *Phys. Rev. E* **58**, 5355-5363 (1998).
 - [6] G. E. Santoro, R. Martoňák, E. Tosatti, R. Car, Theory of Quantum Annealing of an Ising Spin Glass, *Science* **295**, 2427-2430 (2002).
 - [7] A. Das, B. K. Chakrabarti, Colloquium: Quantum annealing and analog quantum computation, *Rev. Mod. Phys.* **80**, 1061-1081 (2008).
 - [8] B. Vlastakis *et al.*, Deterministically Encoding Quantum Information Using 100-Photon Schrödinger Cat States, *Science* **342**, 607-610 (2013).
 - [9] Z. R. Lin *et al.*, Josephson parametric phase-locked oscillator and its application to dispersive readout of superconducting qubits, *Nat. Commun.* **5**, 4480 (2014).
 - [10] H. Okamoto *et al.*, Coherent phonon manipulation in coupled mechanical resonators, *Nat. Phys.* **9**, 480-484 (2013).
 - [11] T. Faust, J. Rieger, M. J. Seitner, J. P. Kotthaus, E. M. Weig, Coherent control of a classical nanomechanical two-level system, *Nat. Phys.* **9**, 485-488 (2013).
 - [12] J. Moser, A. Eichler, J. Güttinger, M. I. Dykman, A. Bachtold, Nanotube mechanical resonators with quality factors of up to 5 million, *Nat. Nanotech.* **9**, 1007-1011 (2014).
 - [13] L. D. Landau, E. M. Lifshitz, *Quantum Mechanics* (Pergamon Press, New York, 1977).
 - [14] U. Leonhardt, *Measuring the Quantum State of Light* (Cambridge Univ. Press, Cambridge, 1997).
 - [15] A coherent state $|\alpha\rangle$ is defined as $a|\alpha\rangle = \alpha|\alpha\rangle$ [14].
 - [16] F. Barahona, On the computational complexity of Ising spin glass models, *J. Phys. A* **15**, 3241-3253 (1982).
 - [17] M. W. Johnson *et al.*, Quantum annealing with manufactured spins, *Nature* **473**, 194-198 (2011).
 - [18] T. Lanting *et al.*, Entanglement in a Quantum Annealing Processor, *Phys. Rev. X* **4**, 021041 (2014).
 - [19] T. F. Ronnow *et al.*, Defining and detecting quantum speedup, *Science* **345**, 420-424 (2014).
 - [20] S. Boixo *et al.*, Evidence for quantum annealing with more than one hundred qubits, *Nat. Phys.* **10**, 218-224 (2014).
 - [21] B. Heim, T. F. Ronnow, S. V. Isakov, M. Troyer, Quantum versus classical annealing of Ising spin glasses, *Science* **348**, 215-217 (2015).
 - [22] S. Utsunomiya, K. Takata, Y. Yamamoto, Mapping of Ising models onto injection-locked laser systems, *Opt. Exp.* **19**, 18091 (2011).
 - [23] Z. Wang, A. Marandi, K. Wen, R. L. Byer, Y. Yamamoto, Coherent Ising machine based on degenerate optical parametric oscillators, *Phys. Rev. A* **88**, 063853 (2013).
 - [24] A. Marandi, Z. Wang, K. Takata, R. L. Byer, Y. Yamamoto, Network of time-multiplexed optical parametric oscillators as a coherent Ising machine, *Nat. Photon.* **8**, 937-942 (2014).
 - [25] The present relaxation is to replace the Ising spins with continuous variables. See Appendix E for details.
 - [26] M. A. Nielsen, I. L. Chuang, *Quantum Computation and Quantum Information* (Cambridge Univ. Press, Cambridge, 2000).
 - [27] T. D. Ladd *et al.*, Quantum computers, *Nature* **464**, 45-53 (2010).
 - [28] D. J. C. MacKay, *Information Theory, Inference and Learning Algorithms* (Cambridge Univ. Press, Cambridge, 2003).
 - [29] M. I. Rabinovich, P. Varona, A. I. Selverston, H. D. I. Abarbanel, Dynamical principles in neuroscience, *Rev. Mod. Phys.* **78**, 1213-1265 (2006).